# Calculation of the $ep \to ep\gamma$ Process in Chiral Perturbation Theory

Xu Wang

September 1, 2025

**Abstract**

This study presents a theoretical calculation of the scattering amplitude for the $ep \to ep\gamma$ process within the framework of Chiral Perturbation Theory (ChPT). We specifically focus on evaluating the tree-level Feynman diagrams up to $O(p^3)$ that contribute to this reaction. The process is of significant interest as it provides valuable insights into the generalized polarizabilities of the nucleon, which are fundamental properties characterizing its response to electromagnetic fields. Our calculations, based on the $O(p^2)$ and $O(p^3)$ nucleon-pion Lagrangians, aim to provide a theoretical prediction for the differential cross-section. By comparing our results with future experimental data, we seek to determine the values of the low-energy constants (LECs) and validate ChPT as an effective low-energy theory of QCD.

## 1 Introduction

The study of electron-proton (ep) scattering provides a crucial window into the internal structure of the proton and the fundamental strong force governed by Quantum Chromodynamics (QCD). At high energies, such scattering can be described by perturbative QCD, but at lower energies, the strong coupling constant becomes large, making a perturbative approach invalid. For these low-energy regimes, effective field theories like Chiral Perturbation Theory (ChPT) offer a powerful and systematic way to analyze the interactions of mesons and nucleons.

In this paper, we focus on the $ep \to ep\gamma$ scattering process, a process of significant interest in low-energy hadron physics. We present a theoretical calculation of the scattering amplitude for this process based on ChPT, with a focus on the contributions from both the Bethe-Heitler (BH) and virtual Compton scattering (VCS) processes. This reaction is a prime candidate for investigating the low-energy structure of the nucleon because it involves the emission of a real photon, which couples directly to the electromagnetic currents of the system. The analysis of this process can provide valuable insights into the generalized polarizabilities of the nucleon, which are fundamental quantities that characterize its response to external electromagnetic fields.

Our theoretical framework is based on ChPT, which provides a rigorous and model-independent approach to calculating physical observables at low energies. We aim to compute the scattering amplitude and differential cross-section for the $ep \to ep\gamma$ process by evaluating all relevant tree-level Feynman diagrams up to $O(p^3)$.

The results of our theoretical calculations will be compared with existing experimental data. This comparison will not only serve as a test of the predictive power of ChPT but also allow us to determine the values of the low-energy constants (LECs) in the ChPT Lagrangian. The determination of these LECs is a critical step, as they encode the complex dynamics of QCD at low energies and are not predicted by the theory itself. By successfully fitting our calculations to experimental data, we can validate our theoretical approach and contribute to a more comprehensive understanding of the strong interaction and the structure of the nucleon.

## 2 Theoretical formalism

### 2.1 Foundamental theory

In the context of the $e(k_1) + p(p_1) \to e(k_2) + p(p_2) + \gamma(k)$ process, experimental data is typically expressed in terms of a set of standard variables, including the virtuality $Q^2$, the Bjorken scaling variable $x_B$, and the momentum transfer $t$. These are defined as follows [1]:

$$Q^2 = -q^2 = -(k_1 - k_2)^2, \quad x_B = Q^2/(2q \cdot p_1), \quad t = (p_2 - p_1)^2 \tag{1}$$

Additionally, an azimuthal angle $\phi$ is used, whose covariant form is defined by [2]:

$$cos\phi = -\frac{g_\perp^{\mu\nu} k_{1\mu} p_{2\nu}}{|k_{1\perp}||p_{2\perp}|}, sin\phi = -\frac{\varepsilon_\perp^{\mu\nu} k_{1\mu} p_{2\nu}}{|k_{1\perp}||p_{2\perp}|} \tag{2}$$

where

$$|k_{1\perp}| = \sqrt{-g_\perp^{\mu\nu} k_{1\mu} k_{1\nu}}, \quad |p_{2\perp}| = \sqrt{-g_\perp^{\mu\nu} p_{2\mu} p_{2\nu}} \tag{3}$$

$$g_\perp^{\mu\nu} = g^{\mu\nu} - \frac{q^\mu p_1^\nu + p_1^\mu q^\nu}{p_1 \cdot q(1+\gamma^2)} + \frac{\gamma^2}{1+\gamma^2}\left(\frac{q^\mu q^\nu}{-q^2} - \frac{p_1^\mu p_1^\nu}{m_N^2}\right) \tag{4}$$

$$\varepsilon_\perp^{\rho\sigma} = \varepsilon^{\mu\nu\rho\sigma} \frac{p_{1\mu} q_\nu}{p_1 \cdot q\sqrt{1+\gamma^2}} \tag{5}$$

where $\gamma = 2x_B m_N/Q, q = k_1 - k_2$.

The differential scattering cross-section is a crucial quantity that directly links theoretical calculations to experimental measurements. The complete differential scattering cross-section for this process is given by [1]:

$$\frac{d^5\sigma}{dQ^2 dx_B dt d\phi d\phi_e} = \frac{\alpha_{QED}^3}{16\pi^2 (s_e - M^2)^2 x_B} \frac{1}{\sqrt{1+\varepsilon^2}} \frac{1}{e^6} |\mathcal{M}|^2 \tag{6}$$

where

$$\varepsilon^2 = 4M^2 x_B^2/Q^2, s_e = (k_1 + p_1)^2 \tag{7}$$

Due to the rotational symmetry of the scattered lepton around the incident axis in the laboratory frame, the scattering result is independent of the angle $\phi_e$. It is therefore common practice to integrate over the $\phi_e$ angle, which simplifies the expression by a factor of $2\pi$, resulting in the following differential scattering cross-section:

$$\frac{d^4\sigma}{dQ^2 dx_B dt d\phi} = \frac{\alpha_{QED}^3}{8\pi (s_e - M^2)^2 x_B} \frac{1}{\sqrt{1+\varepsilon^2}} \frac{1}{e^6} |\mathcal{M}|^2 \tag{8}$$

For the $ep \to ep\gamma$ process, the amplitude $\mathcal{M}$ can be decomposed into the sum of the amplitude from the lepton leg radiation $\mathcal{M}_e$ and the amplitude from the nucleon leg radiation $\mathcal{M}_p$, i.e., $\mathcal{M} = \mathcal{M}_e + \mathcal{M}_p$. Furthermore, the amplitude can be partitioned according to its chiral order:

$$\mathcal{M} = \mathcal{M}^{(1)} + \mathcal{M}^{(2)} + \cdots = (\mathcal{M}_e^{(1)} + \mathcal{M}_e^{(2)} + \dots) + (\mathcal{M}_p^{(1)} + \mathcal{M}_p^{(2)} + \dots) \tag{9}$$

When calculating the squared amplitude, interference terms between different parts also are considered. For example, for the $O(p^1)$ order, the squared amplitude is :

$$|\mathcal{M}^{(1)}|^2 = |\mathcal{M}_e^{(1)}|^2 + |\mathcal{M}_p^{(1)}|^2 + 2\Re(\mathcal{M}_e^{(1)} \mathcal{M}_p^{*(1)}) \tag{10}$$

## 2.2 Chiral Perturbation Theory

Chiral Perturbation Theory (ChPT) is the low-energy effective field theory of QCD that describes the interactions of mesons and nucleons. The results of calculations in ChPT are expanded in terms of a small parameter, $p/(4\pi F)$, where $p$ represents the meson mass or external momentum, and $F$ is the meson decay constant in the chiral limit, with $4\pi F \sim 1\text{GeV}$. The Lagrangian in ChPT is also constructed order by order based on this small parameter. In the process of calculating the $ep \to ep\gamma$ process, we need to use the $\mathcal{O}(p^3)$ Lagrangians, $\mathcal{L}_{\pi N}^{(2)}$ and $\mathcal{L}_{\pi N}^{(3)}$.

First, we give the Lagrangians up to $O(p^3)$ [3]:

$$\begin{aligned}
\mathcal{L}_{\pi N}^{(1)} &= \bar{\Psi}\Big(i\not{D} - m + \frac{g_A}{2}\not{u}\gamma_5\Big)\Psi, \\
\mathcal{L}_{\pi N}^{(2)} &= c_1\langle\chi_+\rangle + \bar{\Psi}\sigma^{\mu\nu}[\frac{c_6}{8m}F_{\mu\nu}^+ + \frac{c_7}{8m}\langle F_{\mu\nu}^+\rangle]\Psi, \text{[1]} \\
\mathcal{L}_{\pi N}^{(3)} &= \bar{\Psi}\Big(\frac{d_6}{2m} i\left[D^\mu, \widetilde{F}_{\mu\nu}^+\right] D^\nu + \text{h.c.}\Big)\Psi + \bar{\Psi}\Big(\frac{d_7}{2m} i\left[D^\mu, \left\langle F_{\mu\nu}^+\right\rangle\right] D^\nu + \text{h.c.}\Big)\Psi,
\end{aligned} \tag{11}$$

where some terms are defined as follows:$D_\mu\Psi = \Big(\partial_\mu + \Gamma_\mu\Big)\Psi$, and

$$\begin{aligned}
\Gamma_\mu &= \frac{1}{2}[u^\dagger(\partial_\mu - ir_\mu)u + u(\partial_\mu - il_\mu)u^\dagger] \\
u^\mu &= i[u^\dagger(\partial_\mu - ir_\mu)u - u(\partial_\mu - il_\mu)u^\dagger] \\
\chi_\pm &= u^\dagger\chi u^\dagger \pm u\chi^\pm u, \\
F_{\mu\nu}^\pm &= uF_{L\mu\nu}u^\dagger \pm u^\dagger F_{R\mu\nu}u \\
F_{L,\mu\nu} &= \partial_\mu l_\nu - \partial_\nu l_\mu - i[l_\mu, l_\nu] \\
F_{R,\mu\nu} &= \partial_\mu r_\nu - \partial_\nu r_\mu - i[r_\mu, r_\nu]
\end{aligned} \tag{12}$$

[1]The definitions of the $c_6$ and $c_7$ terms used here differ slightly from those in Scherer's work [4]. The relationship between the two sets of coefficients is $c_6 = 4m_N c_6'$, $c_7 = m_N(-2c_6' + c_7')$.

Here, the symbols denote the following: $\langle X\rangle$ represents the trace, $\tilde{X} = X - \frac{1}{2}\langle X\rangle$, and h.c. stands for Hermitian conjugate.

Some common terms in the Lagrangian, after expanding the meson fields, are as follows:

$$\begin{aligned}
u &= \mathbb{1} + i\frac{\phi}{2F} - \frac{\phi^2}{8F^2} + \mathcal{O}(\phi^3),\\
\Gamma_\mu &= -ir_\mu + \frac{1}{8F^2}[\phi\partial_\mu\phi - (\partial_\mu\phi)\phi] - \frac{i}{4F^2}\phi r_\mu\phi + \frac{i}{8F^2}\phi^2 r_\mu + \frac{i}{8F^2}r_\mu\phi^2 + \mathcal{O}(\phi^3),\\
u_\mu &= -\frac{1}{F}\partial_\mu\phi + \frac{i}{F}r_\mu\phi - \frac{i}{F}\phi r_\mu + \mathcal{O}(\phi^3),\\
\chi_+ &= 2M^2\mathbb{1} - \frac{1}{F^2}M^2\phi^2 + \mathcal{O}(\phi^3),\\
\chi_- &= -\frac{2i}{F}M^2\phi^2 + \mathcal{O}(\phi^3),\\
F_{L,\mu\nu} &= F_{R,\mu\nu} = -eF_{\mu\nu}Q,\\
F^+_{\mu\nu} &= 2F_{R,\mu\nu} + \frac{1}{2F^2}\phi F_{R,\mu\nu}\phi - \frac{1}{4F^2}\phi^2 F_{R,\mu\nu} - \frac{1}{4F^2}F_{R,\mu\nu}\phi^2 + \mathcal{O}(\phi^3),\\
F^-_{\mu\nu} &= \frac{i}{F}(\phi F_{R,\mu\nu} - F_{R,\mu\nu}\phi) + \mathcal{O}(\phi^3)
\end{aligned} \tag{13}$$

When introducing the photon field, we take

$$r_\mu = l_\mu = -eA_\mu Q, Q = \frac{\mathbb{1} + \tau_3}{2}. \tag{14}$$

Then we can obtain the following Feynman rules:

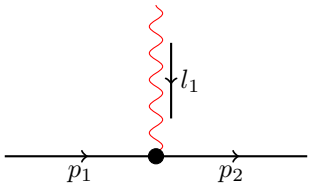


Figure 1: Feynman rules for $ep \to ep\gamma$ up to $O(p^3)$

$$\begin{aligned}
O(p^1) &: -ie\gamma^\mu\\
O(p^2) &: -ie(c_6 + c_7)\gamma^\mu + \frac{ie(c_6 + c_7)}{2m_N}(p_1 + p_2)^\mu\\
O(p^3) &: \frac{ie(d_6 + 2d_7)(p_1 - p_2)^2}{m_N}(p_1 + p_2)^\mu
\end{aligned} \tag{15}$$

The chiral order of the scattering amplitude is calculated using the formula:

$$D = 4L - 2I_\phi - I_N + \sum_{k=1}^{\infty} kN_k^N + \sum_{k=1}^{\infty} 2kN_{2k}^\phi \tag{16}$$

where $L$ is the number of loops, $I_\phi$ is the number of meson internal lines, $I_N$ is the number of nucleon internal lines, $N_k^N$ is the number of nucleon vertices in the Lagrangian, and $N_{2k}^\phi$ is the number of meson vertices.

## 2.3 Feynman Diagram Calculations

The Feynman diagrams for the $ep \to ep\gamma$ process can be broadly divided into two categories: a photon radiating from the lepton (electron) leg, and a photon radiating from the hadron (proton) leg. These two categories can be further subdivided into three distinct diagram structures, as shown in Figure 2.

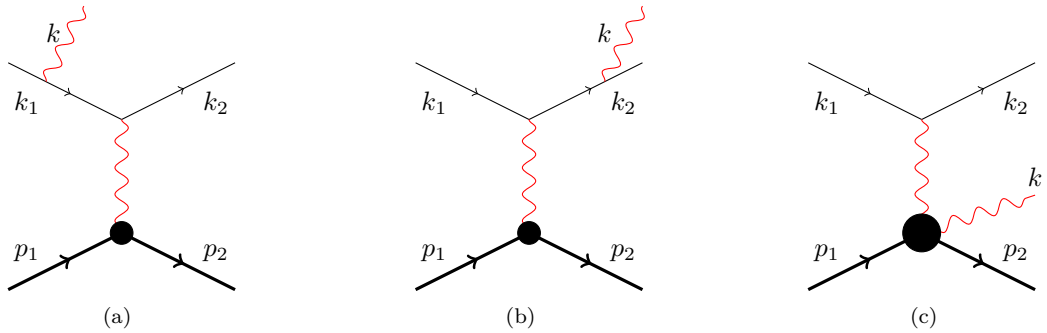


Figure 2: Bremsstrahlung Processes

Figures 2(a) and 2(b) depict the electron bremsstrahlung process, whose amplitudes are primarily described by QED theory, while the proton part is simplified to a "black box" described by form factors. Figure 2(c) describes a virtual Compton scattering process, where a virtual photon interacts with a proton and radiates a real photon. The amplitudes of these three diagrams must be calculated separately and summed to obtain the total scattering amplitude.

For diagrams where the photon radiates from the lepton leg, the amplitude can be decomposed into a leptonic part and a hadronic part. The amplitude $\mathcal{M}_a, \mathcal{M}_b$ for Figure 2(a) and 2(b) can be written as :

$$\begin{aligned}
\mathcal{M}_a &= \bar{u}_1(-ie\gamma^\mu)\frac{i(\not{k}_1 - \not{k} + m_e)}{(k_1-k)^2 - m_e^2}(-ie\gamma^\nu)u_1\frac{-i}{l_1^2}\bar{u}_2\Gamma_\mu u_2\epsilon_\nu^* \\
&= \frac{e^2}{l_1^2}\frac{-1}{(k_1-k)^2 - m_e^2}\bar{u}_1\gamma^\mu(\not{k}_1 - \not{k} + m_e)\gamma^\nu u_1\bar{u}_2\Gamma_\mu u_2\epsilon_\nu^* \\
\mathcal{M}_b &= \bar{u}_1(-ie\gamma^\nu)\frac{i(\not{k} + \not{k}_2 + m_e)}{(k+k_2)^2 - m_e^2}(-ie\gamma^\mu)u_1\frac{-i}{l_1^2}\bar{u}_2\Gamma_\mu u_2\epsilon_\nu^* \\
&= \frac{e^2}{l_1^2}\frac{-1}{(k+k_2)^2 - m_e^2}\bar{u}_1\gamma^\nu(\not{k} + \not{k}_2 + m_e)\gamma^\mu u_1\bar{u}_2\Gamma_\mu u_2\epsilon_\nu^*
\end{aligned} \tag{17}$$

In the expressions above, the hadronic part is described by $\Gamma_\mu$, which is a complex structure containing nucleon form factors. It can generally be decomposed into the Dirac form factor $F_1^N(Q^2)$ and the Pauli form factor $F_2^N(Q^2)$:

$$\Gamma^\mu = F_1^N(Q^2)\gamma^\mu + i\frac{\sigma^{\mu\nu}q_\nu}{2m_N}F_2^N(Q^2) \tag{18}$$

where $Q = p_2 - p_1$. These form factors summarize the influence of the proton's internal structure on electromagnetic interactions, rather than behaving as a simple point particle.

For the virtual Compton scattering process in Figure 2(c), its amplitude $\mathcal{M}_c$ can be written in the following form:

$$\begin{aligned}
\mathcal{M}_c &= \bar{u}_1(-ie\gamma_\mu)u_1\frac{-i}{l_1^2}\bar{u}_2(\Gamma_1^{\mu\nu} + \Gamma_2^{\nu\mu})u_2\epsilon_\nu^* \\
&= \frac{-1}{l_1^2}e\bar{u}_1\gamma_\mu u_1\bar{u}_2(\Gamma_1^{\mu\nu} + \Gamma_2^{\nu\mu})u_2\epsilon_\nu^*
\end{aligned} \tag{19}$$

where $\Gamma_1^{\mu\nu}$ and $\Gamma_2^{\nu\mu}$ represent the complex hadronic part where a virtual photon interacts with the proton and radiates a real photon. For simplification, this hadronic part can be rearranged and defined as the virtual Compton scattering amplitude $M_1^{\mu\nu}$, with the expression $\bar{u}_2(\Gamma_1^{\mu\nu} + \Gamma_2^{\nu\mu})u_2\epsilon_\nu^* \equiv M_1^{\mu\nu}\epsilon_\nu^*$. For ease of calculation, the hadronic amplitude $M_1^{\mu\nu}$ is usually decomposed according to its Lorentz structure :

$$M_1^{\mu\nu} = \sum_i \tilde{u}_2 A_i \Gamma_i^{\mu\nu} u_2$$

where $\Gamma_i^{\mu\nu}$ is a combination of 26 fundamental Lorentz structures, such as $g^{\mu\nu}$, $\gamma^\mu\gamma^\nu$, and various tensors formed from the momenta $k, p_1, p_2$, etc. This decomposition is a common method for handling complex hadronic amplitudes, transforming the problem of calculating the amplitude into one of solving for a series of scalar coefficients $A_i$.

For virtual Compton scattering, calculating at tree level up to $O(p^3)$ order, we obtain the following results (where $p$ denotes that the fermion is a proton). Let the four-momentum of the virtual photon be $l_1 = k + p_2 - p_1$:

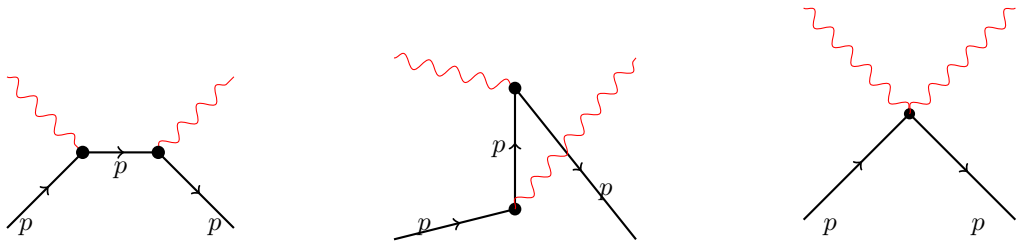


(1) (2) (3)

Figure 3: Virtual Compton Scattering diagrams

Using the derived Feynman rules eq. (15), we can easily obtain the amplitude for Figure 3 as follows:

$$\begin{aligned}\mathcal{M}_1 =& i\bar{u}(p_2, m_N)\cdot\Big(\frac{ie(c_6+c_7)\not{k}\not{\epsilon}^*(k)}{4m_N} - \frac{ie(c_6+c_7)\not{\epsilon}^*(k)\not{k}}{4m_N} + \frac{ie(d_6+2d_7)k^2 p_2\cdot\epsilon^*(k)}{m_N} - ie\not{\epsilon}^*(k)\Big)\\ &\frac{(\not{p}_2+\not{k})+m}{(k+p_2)^2-m^2}\cdot\Big(-\frac{ie(c_6+c_7)\not{l}_1\not{\epsilon}(l_1)}{4m_N} + \frac{ie(c_6+c_7)\not{\epsilon}(l_1)\not{l}_1}{4m_N} - ie\not{\epsilon}(l_1) +\\ &\frac{ie(d_6+2d_7)l_1\cdot\epsilon(l_1)(-l_1\cdot(k+p_2+p_1))}{2m_N} - \frac{ie(d_6+2d_7)l_1^2(-\epsilon(l_1)\cdot(k+p_2+p_1))}{2m_N}\Big)u(p_1, m_N)\end{aligned} \tag{20}$$

$$\begin{aligned}\mathcal{M}_2 =& i\bar{u}(p_2, m_N)\Big(-\frac{ie(c_6+c_7)\not{l}_1\not{\epsilon}(l_1)}{4m_N} + \frac{ie(c_6+c_7)\not{\epsilon}(l_1)\not{l}_1}{4m_N} - ie\not{\epsilon}(l_1)\\ &- \frac{ie(d_6+2d_7)l_1\cdot\epsilon(l_1)(l_1\cdot(p_1+p_2-k))}{2m_N} + \frac{ie(d_6+2d_7)l_1^2(\epsilon(l_1)\cdot(p_1+p_2-k))}{2m_N}\Big)\cdot\frac{(\not{p}_1-\not{k})+m}{(k-p_1)^2-m^2}\cdot\\ &\Big(\frac{ie(c_6+c_7)\not{k}\not{\epsilon}^*(k)}{4m_N} - \frac{ie(c_6+c_7)\not{\epsilon}^*(k)\not{k}}{4m_N} + \frac{ie(d_6+d_7)k^2(p_1\cdot\epsilon^*(k))}{m_N} - ie\not{\epsilon}^*(k)\Big)u(p_1, m_N)\end{aligned} \tag{21}$$

$$\mathcal{M}_3 = \bar{u}(p_2, m_N)\frac{ie^2(d_6+2d_7)}{m_N}([l_1\cdot\epsilon(l_1)][l_1\cdot\epsilon^*(k)] - k^2[\epsilon(l_1)\cdot\epsilon^*(k)] - l_1^2[\epsilon(l_1)\cdot\epsilon^*(k)])u(p_1, m_N) \tag{22}$$

These initial expressions contain higher-order terms that need to be truncated according to the chiral power counting method eq. (16). The document explicitly states that since the highest order of the vertices is $O(p^3)$, the highest-order amplitude can reach $O(p^5)$. To maintain consistency in the calculation, terms higher than $O(p^3)$ must be removed.

After truncation and rearrangement, the results for each order of amplitude are as follows :

| | $\gamma^\mu\gamma^\nu$ | $\gamma^\mu\gamma^\nu \not{k}$ | $k^\mu\gamma^\nu$ | $k^\mu\gamma^\nu \not{k}$ |
|---|---|---|---|---|
| $\mathcal{M}^{(1)\mu\nu}$ | $0$ | $\frac{ie^2}{m_N^2-s_1}+\frac{ie^2}{m_N^2-t_1}$ | $0$ | $-\frac{-2ie^2}{m_N^2-s_1}$ |
| $\mathcal{M}^{(2)\mu\nu}$ | $0$ | $\frac{2m_NA}{m_N^2-s_1}+\frac{2A}{m_N^2-t_1}$ | $-2A$ | $-\frac{4A}{m_N^2-s_1}$ |
| $\mathcal{M}^{(3)\mu\nu}$ | $0$ | $\frac{B(3m_N^2+s_1)}{4(m_N^2-s_1)}+\frac{B(3m_N^2+t_1)}{4(m_N^2-t_1)}$ | $\frac{C(2m_N^2-s_1-t_1-t_2)}{m_N}-B$ | $-\frac{B(3m_N^2+s_1)}{2(m_N^3-m_Nt_1)}$ |
| | $p_1^\mu\gamma^\nu$ | $p_1^\mu\gamma^\nu \not{k}$ | $p_2^\mu\gamma^\nu$ | $p_2^\mu\gamma^\nu \not{k}$ |
| $\mathcal{M}^{(1)\mu\nu}$ | $\frac{2ie^2}{m_N^2-s_1}$ | $0$ | $0$ | $0$ |
| $\mathcal{M}^{(2)\mu\nu}$ | $\frac{4m_NA}{m_N^2-s_1}$ | $-\frac{A}{2(m_N^2-s_1)}+\frac{A}{2(m_N^2-t_1)}$ | $0$ | $-\frac{A}{2(m_N^2-s_1)}-\frac{A}{2(m_N^2-t_1)}$ |
| $\mathcal{M}^{(3)\mu\nu}$ | $-\frac{B(7m_N^2+s_1)}{4(m_N^2-s_1)}-\frac{1}{4}B$ | $\frac{C(m_N^2-t_1-t_2)-Bm_N^2}{2(m_N^3-m_Ns_1)}+\frac{Bm_N^2-C(m_N^2-s_1-t_2)}{2(m_N^3-m_Nt_1)}$ | $\frac{1}{2}B$ | $\frac{C(3m_N^2-2s_1-t_1-t_2)-Bm_N^2}{2(m_N^3-m_Ns_1)}+\frac{C(m_N^2-s_1-t_2)-Bm_N^2}{2(m_N^3-m_Nt_1)}$ |
| | $g^{\mu\nu}$ | $g^{\mu\nu} \not{k}$ | $p_1^\nu\gamma^\mu$ | $p_1^\nu\gamma^\mu \not{k}$ |
| $\mathcal{M}^{(1)\mu\nu}$ | $0$ | $0$ | $\frac{2ie^2}{m_N^2-t_1}$ | $0$ |
| $\mathcal{M}^{(2)\mu\nu}$ | $0$ | $-\frac{A}{2(m_N^2-s_1)}-\frac{A}{2(m_N^2-t_1)}$ | $\frac{m_NA}{m_N^2-t_1}$ | $\frac{A}{m_N^2-t_1}$ |
| $\mathcal{M}^{(3)\mu\nu}$ | $\frac{1}{2}B$ | $\frac{C(m_N^2-t_1-t_2)-Bm_N^2}{2(m_N^3-m_Ns_1)}+\frac{C(3m_N^2-s_1-2t_1-t_2)-Bm_N^2}{(2m_N^3-m_Nt_1)}$ | $0$ | $\frac{C(m_N^2-t_1-t_2)}{m_N^3-m_Ns_1}+\frac{Bm_N}{m_N^2-t_1}$ |
| | $k^\mu p_1^\nu$ | $k^\mu p_1^\nu \not{k}$ | $p_1^\mu p_1^\nu$ | $p_1^\mu p_1^\nu \not{k}$ |
| $\mathcal{M}^{(1)\mu\nu}$ | $\frac{2ie^2}{m_N^2-s_1}$ | $0$ | $0$ | $0$ |
| $\mathcal{M}^{(2)\mu\nu}$ | $\frac{m_NA}{m_N^2-s_1}$ | $\frac{A}{m_N^2-s_1}$ | $-\frac{A}{m_N^2-t_1}$ | $0$ |
| $\mathcal{M}^{(3)\mu\nu}$ | $0$ | $\frac{Bm_N}{m_N^2-s_1}$ | $\frac{C}{m_N}+\frac{C(m_N^2-s_1-t_2)}{m_N^3-m_Nt_1}$ | $\frac{C(m_N^2-t_1-t_2)}{m_N^3-m_Ns_1}-\frac{B}{2(m_N^2-t_1)}$ |
| | $p_2^\mu p_1^\nu$ | $p_2^\mu p_1^\nu \not{k}$ | $p_2^\nu\gamma^\mu$ | $p_2^\nu\gamma^\mu \not{k}$ |
| $\mathcal{M}^{(1)\mu\nu}$ | $0$ | $0$ | $0$ | $0$ |
| $\mathcal{M}^{(2)\mu\nu}$ | $-\frac{A}{m_N^2-s_1}$ | $0$ | $\frac{A}{m_N^2-t_1}$ | $0$ |
| $\mathcal{M}^{(3)\mu\nu}$ | $\frac{C}{m_N}+\frac{C(m_N^2-t_1-t_2)}{m_N^3-m_Ns_1}$ | $\frac{B}{2(m_N^2-s_1)}$ | $-\frac{C}{m_N}-\frac{C(m_N^3-s_1-t_2)}{m_N^3-m_Nt_1}$ | $\frac{B}{2(m_N^2-t_1)}$ |
| | $k^\mu p_2^\nu$ | $k^\mu p_2^\nu \not{k}$ | $p_1^\mu p_2^\nu$ | $p_1^\mu p_2^\nu \not{k}$ |
| $\mathcal{M}^{(1)\mu\nu}$ | $0$ | $0$ | $0$ | $0$ |
| $\mathcal{M}^{(2)\mu\nu}$ | $-\frac{3A}{m_N^2-s_1}$ | $0$ | $-\frac{A}{m_N^2-s_1}$ | $0$ |
| $\mathcal{M}^{(3)\mu\nu}$ | $\frac{C}{m_N}+\frac{C(m_N^2-t_1-t_2)}{m_N^3-m_Ns_1}-\frac{2Bm_N}{m_N^2-s_1}$ | $\frac{C}{2(m_N^2-s_1)}$ | $-\frac{C}{m_N}+\frac{C(3m_N^2-2s_1-t_1-t_2)}{m_N^3-m_Ns_1}$ | $\frac{B}{2(m_N^2-s_1)}$ |
| | $p_2^\mu p_2^\nu$ | $p_2^\mu p_2^\nu \not{k}$ | | |
| $\mathcal{M}^{(1)\mu\nu}$ | $0$ | $0$ | | |
| $\mathcal{M}^{(2)\mu\nu}$ | $-\frac{A}{m_N^2-t_1}$ | $0$ | | |
| $\mathcal{M}^{(3)\mu\nu}$ | $-\frac{C}{m_N}+\frac{C(3m_N^2-s_1-2t_1-t_2)}{m_N^3-m_Nt_1}$ | $-\frac{B}{2(m_N^2-t_1)}$ | | |

Table 1: Virtual Compton Scattering amplitudes

where $A = ie^2(c_6 + c_7), B = ie^2(c_6 + c_7)^2, C = ie^2(d_6 + 2d_7)$.

It is important to note a key detail here, which is the use of mass in the proton propagator. The $c_1$ term in the Lagrangian introduces a mass correction, i.e., $m \to m_2 = m - 4c_1M^2$ . However, $m_2 - m_N \sim O(p^3)$, and this mass difference only appears in $O(p^3)$ loop diagram calculations. Since this is a tree diagram calculation, the propagator mass can be directly replaced with the true nucleon mass $m_N$.

# 3 Experimental Fitting

To compare experimental results with theoretical calculations, we need to ensure the variables are consistent. We can easily convert $s, s_1, s_2, t_1, t_2$ into functions of $Q^2, x_B, t, \phi$ and $E_k$, where $E_k$ is the energy of the incident lepton in the lab frame.

$$s = m_e^2 + m_N^2 + 2m_N E_k \tag{23}$$

$$s_1 = -\frac{-Q^2 - m_N^2 x_B + Q^2 x_B}{x_B} \tag{24}$$

$$t_1 = -\frac{Q^2 - m_N^2 x_B + t x_B}{x_B} \tag{25}$$

$$t_2 = t \tag{26}$$

As for $s_2$, its numerical relationship with $Q^2, x_B, t, \phi, E_k$ can be easily derived.

The experimental data has been summarized in Tables 7, 8, 12, and 13 of [1].

Here, we present the individual fitting results for each table, as well as the overall fitting results when all tables are combined.

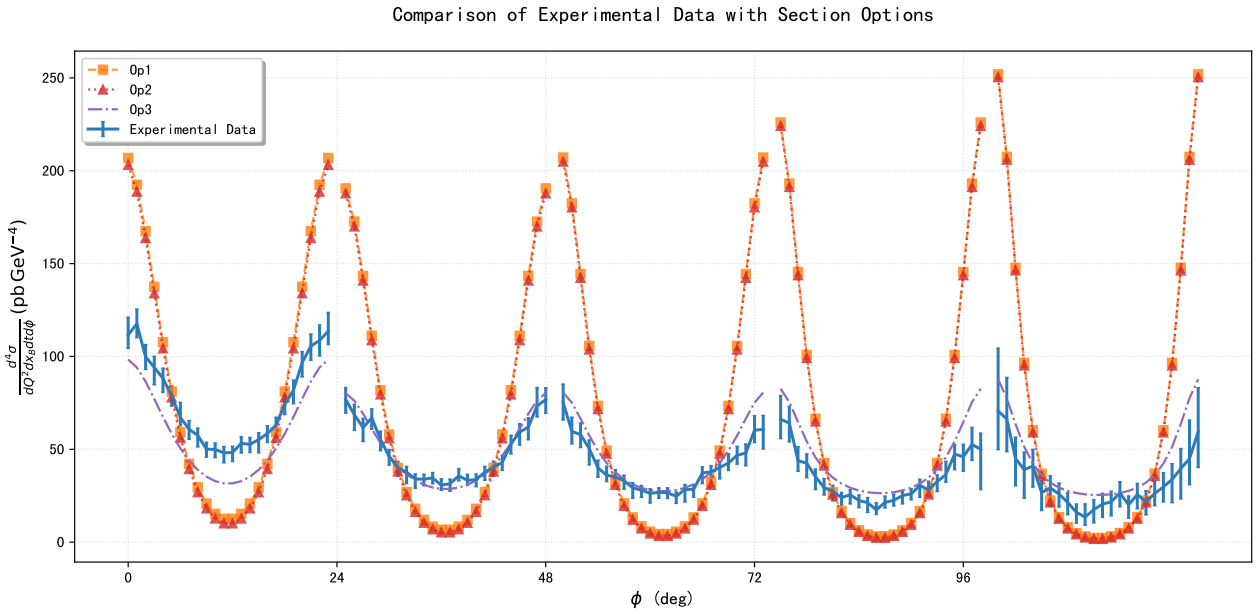


Figure 4: Fit Results for Table 7 data

Table 2: Fitted parameters $\alpha_1 = c_6 + c_7$ and $\alpha_2 = d_6 + 2d_7$, and $\chi^2/dof$ values for different orders for Table 7 data

| | $O(p^2)$ | $O(p^3)$ |
|---|---|---|
| $\alpha_1 = c_6 + c_7$<br>$\alpha_2 = d_6 + 2d_7$ | $\alpha_1 = -0.2149 \pm 0.0720$ | $\alpha_1 = 0.2867 \pm 0.0161$<br>$\alpha_2 = -1.2580 \pm 0.0172$ |
| $\chi^2$/dof | 61.13 | 3.54 |

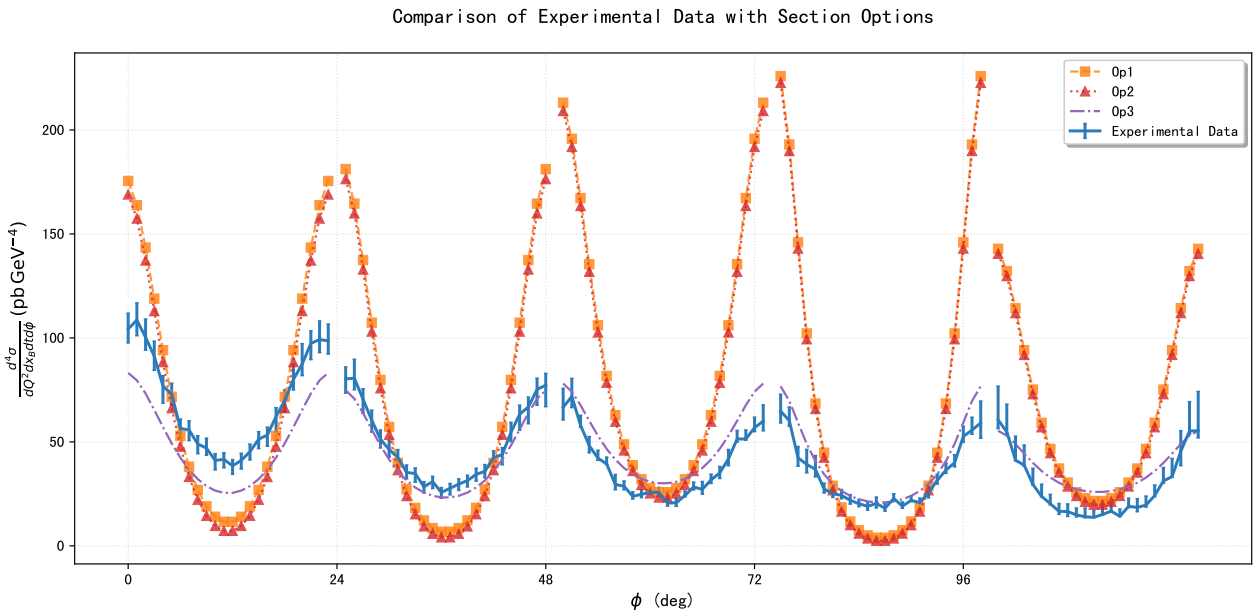


Figure 5: Fit Results for Table 8 data

Table 3: Fitted parameters $\alpha_1 = c_6 + c_7$ and $\alpha_2 = d_6 + 2d_7$, and $\chi^2/dof$ values for different orders for Table 8 data

| | $O(p^2)$ | $O(p^3)$ |
|---|---|---|
| $\alpha_1 = c_6 + c_7$<br>$\alpha_2 = d_6 + 2d_7$ | $\alpha_1 = -0.3437 \pm 0.0636$ | $\alpha_1 = 0.1089 \pm 0.0159$<br>$\alpha_2 = -1.1365 \pm 0.0172$ |
| $\chi^2$/dof | 71.62 | 5.97 |

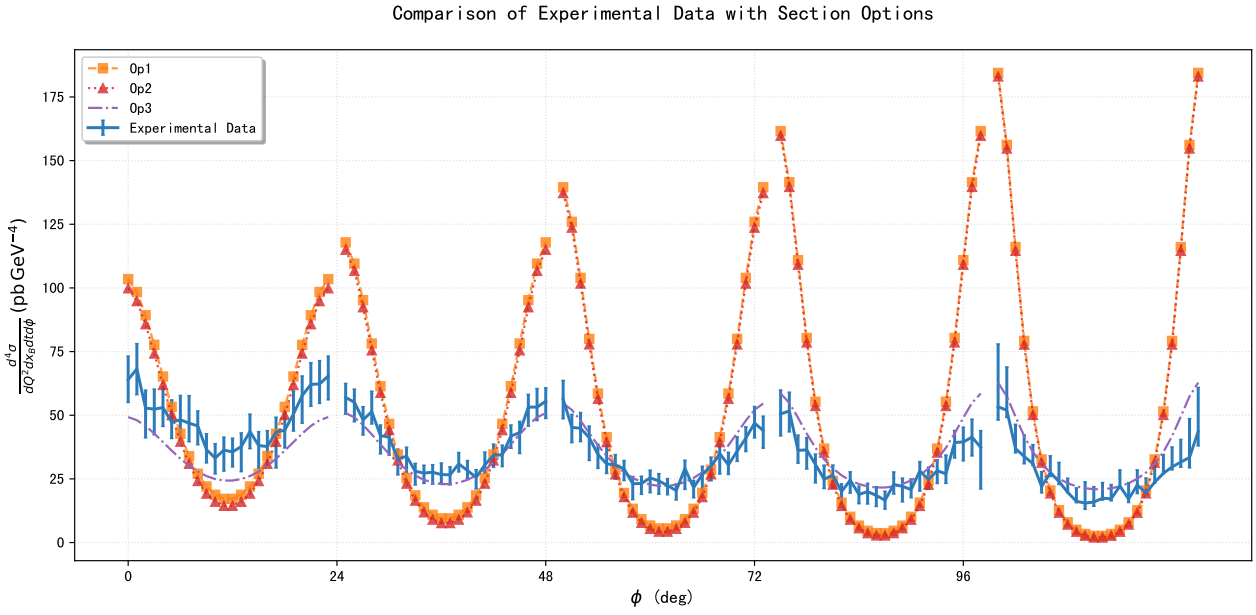


Figure 6: Fit Results for Table 12 data

Finally, the results for the global fit of all data are as follows :

Table 4: Fitted parameters $\alpha_1 = c_6 + c_7$ and $\alpha_2 = d_6 + 2d_7$, and $\chi^2/dof$ values for different orders for Table 12 data

| | $O(p^2)$ | $O(p^3)$ |
|---|---|---|
| $\alpha_1 = c_6 + c_7$<br>$\alpha_2 = d_6 + 2d_7$ | $\alpha_1 = -0.2852 \pm 0.1147$ | $\alpha_1 = 0.1961 \pm 0.0212$<br>$\alpha_2 = -1.1721 \pm 0.0241$ |
| $\chi^2$/dof | 30.95 | 1.38 |

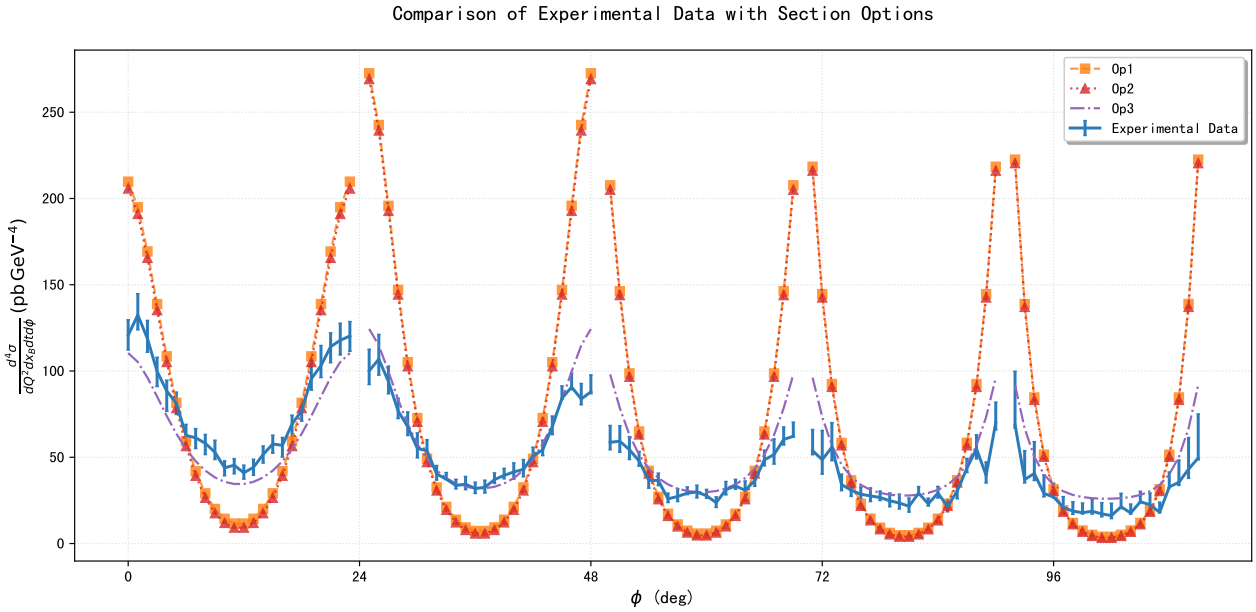


Figure 7: Fit Results for Table 13 data

Table 5: Fitted parameters $\alpha_1 = c_6 + c_7$ and $\alpha_2 = d_6 + 2d_7$, and $\chi^2/dof$ values for different orders for Table 13 data

| | $O(p^2)$ | $O(p^3)$ |
|---|---|---|
| $\alpha_1 = c_6 + c_7$<br>$\alpha_2 = d_6 + 2d_7$ | $\alpha_1 = -0.1577 \pm 0.0585$ | $\alpha_1 = 0.3158 \pm 0.0220$<br>$\alpha_2 = -1.2067 \pm 0.0234$ |
| $\chi^2$/dof | 32.52 | 2.50 |

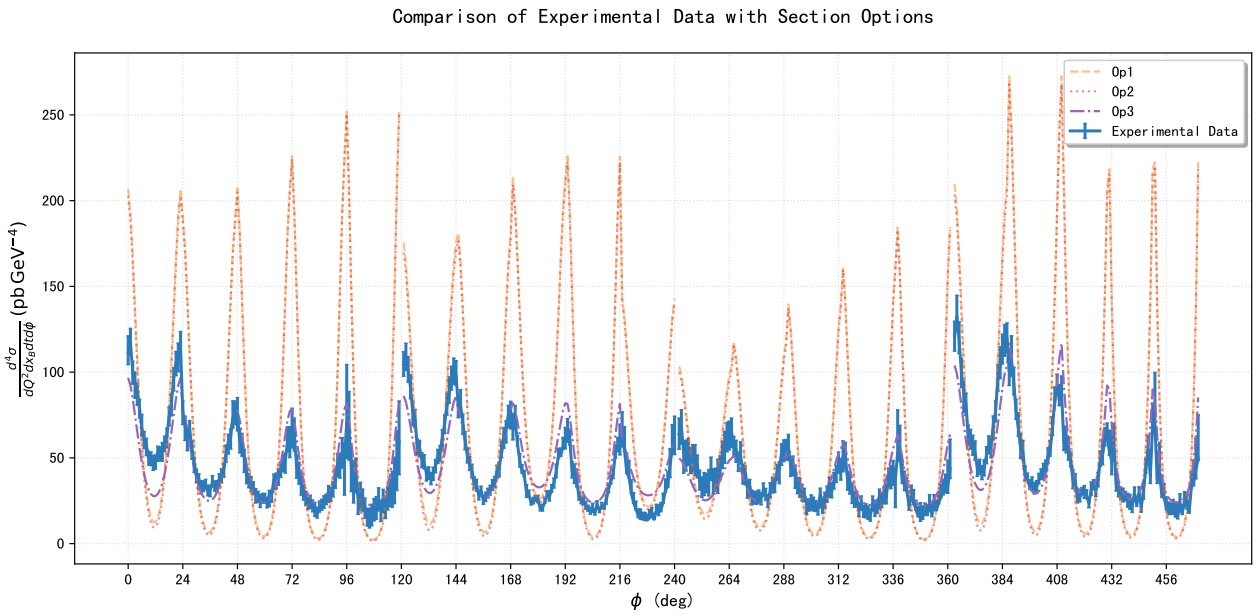


Figure 8: Global fit results for all data

Table 6: Fitted parameters $\alpha_1 = c_6 + c_7$ and $\alpha_2 = d_6 + 2d_7$, and $\chi^2/dof$ values for different orders for all data

| | $O(p^2)$ | $O(p^3)$ |
|---|---|---|
| $\alpha_1 = c_6 + c_7$<br>$\alpha_2 = d_6 + 2d_7$ | $\alpha_1 = -0.2786 \pm 0.0368$ | $\alpha_1 = 0.2114 \pm 0.0090$<br>$\alpha_2 = -1.1951 \pm 0.0098$ |
| $\chi^2$/dof | 49.35 | 3.65 |

# 4 Conclusion

This study presents a theoretical calculation of the scattering amplitude for the $ep \to ep\gamma$ process within the framework of Chiral Perturbation Theory (ChPT). We specifically focused on evaluating the tree-level Feynman diagrams up to $O(p^3)$ that contribute to this reaction. The process is of significant importance as it provides valuable insights into the generalized polarizabilities of the nucleon, which are fundamental properties characterizing its response to electromagnetic fields.

Our calculations, based on the $O(p^2)$ and $O(p^3)$ nucleon-pion Lagrangians, aim to provide a theoretical prediction for the differential cross-section. By comparing our results with future experimental data, we aim to determine the values of the low-energy constants (LECs) and validate ChPT as an effective low-energy theory of QCD. The determination of LECs is crucial because they encode the complex dynamics of QCD at low energies, which are not predictable by the theory itself. By successfully fitting our calculations to experimental data, we can validate our theoretical approach and contribute to a more comprehensive understanding of strong interactions and nucleon structure.

# References


[1] M Defurne, M Amaryan, KA Aniol, M Beaumel, H Benaoum, P Bertin, M Brossard, A Camsonne, J-P Chen, E Chudakov, et al. E00-110 experiment at jefferson lab hall a: Deeply virtual compton scattering off the proton at 6 gev. *Physical Review C*, 92(5):055202, 2015.

[2] Alessandro Bacchetta, Umberto D'Alesio, Markus Diehl, and C. Andy Miller. Single-spin asymmetries: The trento conventions. *Phys. Rev. D*, 70:117504, Dec 2004.

[3] Nadia Fettes, Ulf-G Meißner, Martin Mojžiš, and Sven Steininger. The chiral effective pion-nucleon lagrangian of order p4. *Annals of Physics*, 283(2):273–307, 2000.

[4] Stefan Scherer and Matthias R. Schindler. A chiral perturbation theory primer, 2005.